ChemistrySelect

Research Article
doi.org/10.1002/slct.202501307

Chemistry Europe
European Chemical Societies Publishing

www.chemistryselect.org

Enhancing the Electrochemical Properties of Metal Deposits in Autocatalytic Copper Deposition Baths Containing Polyols

Suseela Jayalakshmi,[a] Raja Venkatesan,*[b, c] Palanivelu Balaramesh,[d] Simon Deepa,[a] Maher M. Alrashed,*[e] and Seong-Cheol Kim*[c]

This paper reveals the impact of pH and the number of hydroxide groups in an environmentally friendly copper deposition bath using polyhydroxylic chelators using dimethylamine borane (DMAB) as a reductant and potassium hydroxide as a pH adjuster at room temperature (28 ± 2 °C). Glycerol, erythritol, xylitol, and sorbitol are examples of monosaccharide polyols having tri, tetra, penta, and hexa hydroxylic groups in their structures were used as an environmentally benign complexing agent in the methane sulphonic acid (MSA) solvated deposition bath. The study demonstrated that, in addition to the hydroxide groups in the polyols, the pH of the electroless bath is a critical factor in copper deposition. The impact of temperature and pH on the rate of deposition of the bath was examined. Atomic absorption spectroscopy and X-ray diffraction studies was used to examine the surface and structural properties of the deposits and Tafel, electrochemical impedance, and cyclic voltammetry (CV) were used to examine the electrochemical properties of the polyol chelated deposition bath.

1. Introduction

Silver, coated as a film, was the first metal to undergo electroless deposition.[1] However, the scientific explanation of this process was provided by German chemist Justus Von Liebig in 1835. Later, in 1947, Harold Narcus works on "copper reduction on non-conductors" initiated the study of electroless copper on nonconductive surfaces.[2] By the mid-1950s, electroless copper plating gained commercial acceptance with the development of plated through-hole (PTH) printed circuit boards (PCBs).[3–5] These coatings provide excellent properties, including good absorptivity, high hardness, uniform distribution, and strong adhesion.[6,7]

Among various deposition techniques, the simplest and most widely used method is dip coating, where a substrate is dipped into a solution containing metal salts and reducing agents to enable electroless deposition.[8] Dip coating is favored for its ease of processing, cost-effectiveness, and high-quality coatings.[9,10] Alternative deposition methods, such as spin coating, spraying, and meniscus coating can be useful for specific applications. Industrial applications of dip coating, date back to pioneering research at Schott in the 1940s. Since the late 1950s, this method has been employed in the manufacture of automotive rearview mirrors, as well as large-area optical coatings such as sun control and antireflective glasses.[11] Many traditional electroless deposition baths incorporate hazardous substances, including heavy metal ions and complexing agents, which present environmental challenges and necessitate stringent waste management. Additionally, elevated operating temperatures can further intensify toxicity, exacerbating their environmental impact.

This study focuses on copper methanesulphonate electroless baths containing polyhydroxylic alcohols, which serve as eco-friendly chelators in an alkaline medium. These chelators replace the traditionally used EDTA, whose biodegradability has been questioned in recent years.[12,13] The electroless deposition baths were prepared using four different polyhydroxylic complexing agents-glycerol, erythritol, xylitol, and sorbitol forming four distinct deposition baths.[14–18] The reducing agent, DMAB, was used in combination with potassium hydroxide to adjust the pH and optimize the baths. The optimal pH of each bath was determined based on the nature of the complexing agent, with values set at 11.50, 11.25, 11.00, and 10.75 for glycerol, erythritol, xylitol, and sorbitol, respectively. All baths were maintained at a room temperature of 28 ± 2 °C. The operational temperature of the commonly used electroless deposition bath lies in the range of

[a] S. Jayalakshmi, S. Deepa
Department of Chemistry, School of Basic Sciences, Vels Institute of Science, Technology and Advanced Studies, Chennai 600117, Tamil Nadu, India

[b] R. Venkatesan
Department of Biomaterials, Saveetha Dental College and Hospitals, SIMATS, Saveetha University, Chennai 600077, Tamil Nadu, India
E-mail: rajavenki@yu.ac.kr

[c] R. Venkatesan, S.-C. Kim
School of Chemical Engineering, Yeungnam University, 280 Daehak-Ro, Gyeongsan 38541, Republic of Korea
E-mail: sckim07@ynu.ac.kr

[d] P. Balaramesh
Department of Chemistry, R.M.K. Engineering College, Chennai 601206, Tamil Nadu, India

[e] M. M. Alrashed
Chemical Engineering Department, College of Engineering, King Saud University, P.O. Box 800, Riyadh 11421, Saudi Arabia
E-mail: mabdulaziz@ksu.edu.sa

Supporting information for this article is available on the WWW under https://doi.org/10.1002/slct.202501307

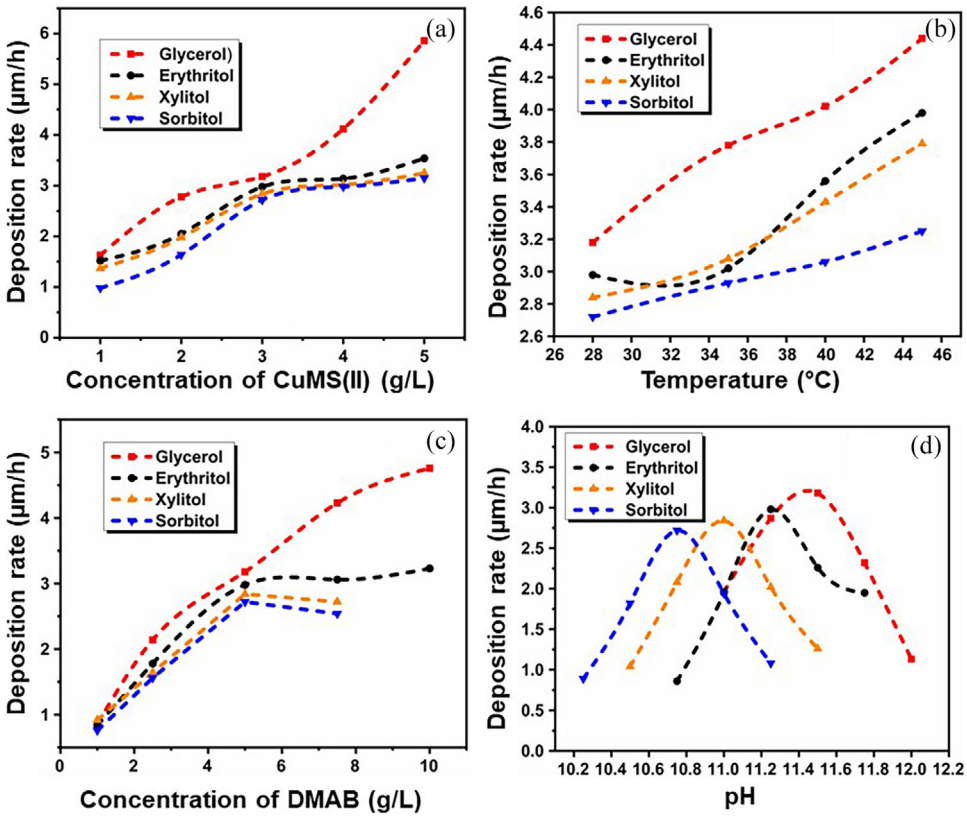

Figure 1. Effect of concentration of copper on electroless deposition baths; (a) CuMS(II) ion contacting salt, (b) Temperature, (c) DMAB, and (d) pH.

45–70 °C. But the current study focuses on an operating temperature of 28 ± 2 °C promising a less toxic eco-friendly, excellent, precise, and uniform smooth deposits of copper, hence finds unique from the existing electroless copper deposition baths. The use of methanesulphonic acid in the bath solution plays a crucial role in producing high-quality deposits with uniform distribution.[19–22] In an alkaline solution, the reductant DMAB readily dissociates, forming an intermediate hydroxytrihydroborate anion, which undergoes oxidation, leading to the release of hydrogen gas. The two half-reactions occurring in an electroless deposition bath utilizing DMAB are as follows:

Cathodic reaction,

$$Cu^{2+} + 2e^{-} \rightarrow Cu$$

Anodic reaction,

$$(CH_3)_2NH.BH_3 + OH^{-} \rightarrow BH_3OH^{-} + (CH_3)_2NH$$

$$BH_3OH^{-} + 3OH^{-} \rightarrow B(OH)_4^{-} + 3H_2 + 3e^{-}$$

2. Results and Discussion

The concentration of the bath components, reducing agent, the temperature and the pH plays a major part in the stability of the bath and in the texture of the copper deposits.[23] The balance between each components distinct function, dictates the bath stability, quality, and rate of plating. For example, chelating agents that are naturally occurring polyhydroxylic compounds are favored due to their homogeneous deposit formation and biodegradability. The final electroless copper deposit, which is extensively utilized in many applications, such as semiconductor production, integrated circuits, and ornamental items, must have the appropriate qualities, and this can only be achieved by optimizing these components. The electroless deposition baths were optimized through a trial-and-error method considering the stability and the deposition rate of the bath.[24]

In an electroless deposition bath containing 100 mL solution, the copper ion concentration is varied from 1.0 to 5.0 g/L, where the maximum deposition is found at a concentration of 3.0 g/L. Therefore, the bath is optimized at this concentration where the stability is found to be more comparing other deposition bath as shown in Table S2 and Figure 1a. In Figure 1b,c, the effect of temperature and the effect of reducing agents in an autocatalytic deposition bath have been shown, where it clearly indicates that the Electroless bath containing varying complexing agent have shown results till an optimum temperature and optimum concentration of reductants is achieved. With further rise in temperature and the reductants, the bath becomes unstable and decomposes which badly affect the deposition process.[25]

The glycerol, erythritol, xylitol, and sorbitol contained baths were optimized at a pH of 11.50, 11.25, 11.00, and 10.75, respectively. It was observed that the baths containing glycerol, erythritol, xylitol, and sorbitol containing tri, tetra, penta, and hexa hydrox-

Table 1. Surface and electrochemical characteristics of the electroless deposition baths.

S. No	Electroless Deposition Baths	AFM Roughness Value (nm)	XRD Crystallite Size (nm)	Cyclic Voltammetry E_{pa-1} Values (V)	Cyclic Voltammetry I_{pa-1} Values (A)	Tafel I_{corr} (mA)	Deposition Rate (μm/h)	Impedance Charge Transfer Resistance (R_t) (mΩ/cm^2) R_1	R_2	R_3
1.	Glycerol	23.411	17.82	−0.2695	3.303×10^{-4}	235.3	3.115	11.24	11.04	67.86
2.	Erythritol	38.798	20.17	−0.2885	4.956×10^{-4}	214.9	2.845	9.01	7.03	74.80
3.	Xylitol	49.618	22.22	−0.3161	1.497×10^{-4}	184.8	2.446	6.26	6.56	85.52
4.	Sorbitol	60.095	29.89	−0.3400	1.190×10^{-4}	177.8	2.354	8.19	6.89	94.82

ylic groups, respectively, were optimized at a pH in an order, where the pH decreases from glycerol to sorbitol. In general, the deposition rate of an electroless deposition bath increases with the increase in pH, reaches a maximum and then decreases. In that concern, the glycerol bath which is optimized at a higher pH than all other three electroless deposition baths, has shown better deposition rate. The glycerol bath has shown a maximum deposition rate of 3.18 μm/h at a pH of 11.50 which is high compared to the pH of other three deposition baths with a deposition rate of 2.98, 2.84, and 2.72 μm/h for erythritol, xylitol, and sorbitol, respectively. The significance of pH in electroless deposition baths is well established, as it directly affects the deposition rate, bath stability, and the quality of the final coating. An elevated pH can enhance the reduction reaction, facilitating the formation of metal nuclei, whereas a lower pH may inhibit the process or even compromise bath stability. This study distinctly highlights the role of pH in shaping bath characteristics, in addition to the steric hindrance introduced by the increasing presence of hydroxide groups.[26,27] The pH dependence of the deposition bath on the rate of deposition are shown in Table S3 and Figure 1d.

The structural properties of copper deposits were evaluated by examining the peaks at the (111), (200), and (220) planes. As shown in Table 1 and Figure 2, copper typically exhibits a preferred orientation along the (111) plane within its FCC structure. However, in our study, the combined effects of high conductivity and the solubility of biodegradable methanesulphonic acid have shifted the orientation from the lower (111) plane to the higher (200) plane.

The physical and the mechanical characteristics of the copper deposits is studied using the atomic absorption spectroscopy. Smooth deposits of copper are obtained whose roughness value is obtained from the AFM studies. Smoothness and roughness have an inverse relationship. The findings of the study also helped explain why the glycerol-containing bath produced smooth deposits with a roughness value of 23.411 nm, which is significantly lower than that of the other three deposition baths. Table 1 and Figure 3 shows the topography and the roughness value of the copper deposits of all the copper methane sulphonate baths.

The electrochemical characteristics of the bath were studied using the cyclic voltammetry (Figure 4), Tafel, and electrochemical impedance studies.[28,29] The kinetics of electrochemical reactions at the electrode surfaces can be studied by the cyclic

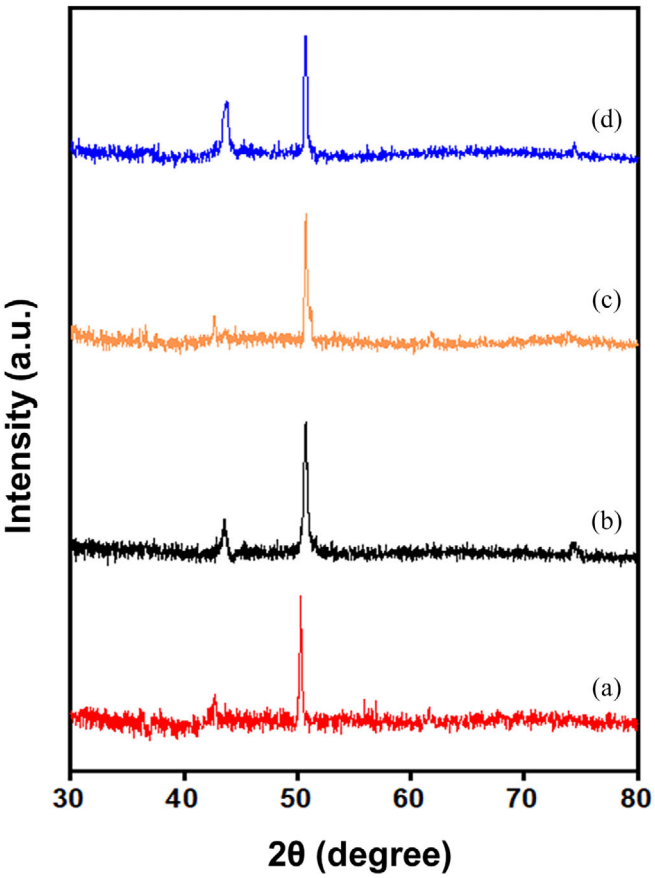

Figure 2. XRD pattern of copper deposits; (a) glycerol, (b) erythritol, (c) xylitol, and (d) sorbitol baths.

voltammetry technique. Figures 5a,b shows the results obtained from the electrochemical studies of all the four electroless baths. The anodic peak potential (E_{pa-1} values) obtained from the cyclic voltammetry for glycerol is found to be −0.2695 V, while that of erythritol, xylitol, and sorbitol is found to be −0.2885, −0.3161, and −0.3400 V, respectively. The anodic peak potential indicates the ease with which the analyte undergoes oxidation. A lower peak potential suggests a more favorable oxidation process, which is been shown by the glycerol contained electroless bath. Similarly, the corrosion current (I_{corr}) obtained from Tafel studies and the resistance shown by the impedance studies for glycerol was found to be 235.3 mA and 67.86 mΩ/cm^2 which clearly indicates that among the four electroless baths, the bath containing

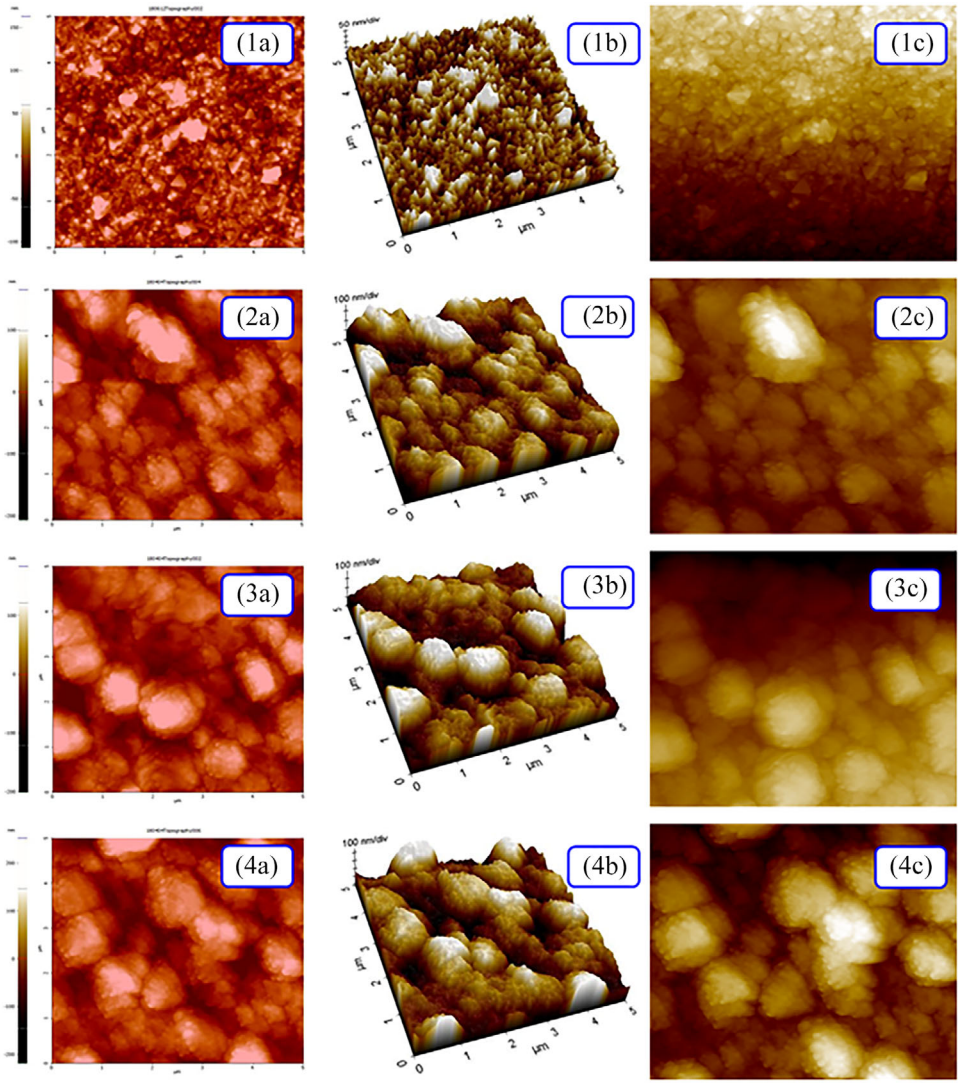

Figure 3. AFM images of copper deposits; (a) Topography of copper deposits (b) 3-D image, and (c) surface area; (1) glycerol, (2) erythritol, (3) xylitol, and (4) sorbitol baths.

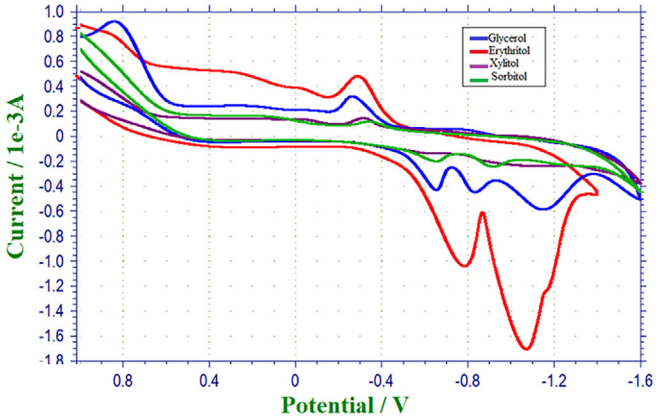

Figure 4. Cyclic voltammogram of electroless copper methanesulphonate deposition baths.

glycerol as the chelator gave better results when compared to all the other three electroless baths.[30]

In general, the electrochemical characteristics of the work clearly indicates that all the four polyhydroxy chelated baths have shown better deposition rate and corrosion resistance at room temperature rather than the conventional chelated deposition baths. The corrosion resistance enhances the longevity and reliability of coated surfaces making them ideal for electronic components, printed circuit boards (PCBs), and industrial machinery and high deposition rates improves manufacturing efficiency, reducing processing time and costs.

3. Conclusion

In this study, the electroless deposition baths were analyzed, and the results were concluded;

- The chelators in the study are arranged based on the number of hydroxide groups present in them. The increase in the number of hydroxides in the bath decreases the performance of the bath which is evident from the results obtained.

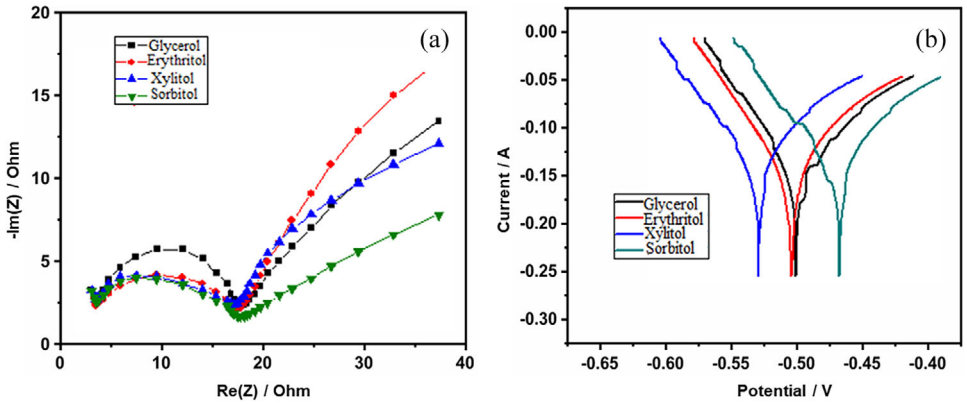

Figure 5. The electroless copper methanesulphonate baths; (a) Tafel polarization curves and (b) Nyquist diagram.

- The optimization pH of the electroless deposition bath dropped from glycerol to sorbitol. The glycerol contained bath which is optimized at a higher pH than the other baths, has exhibited best performance than the other three baths attributing the fact that apart from the number of hydroxides in the bath, the pH also plays an important role in the bath stability and deposition.
- The results from the AFM analysis reported that among all the four chelators, glycerol, erythritol, xylitol, and sorbitol, the bath containing glycerol has given the best textured, uniformly distributed deposits than the deposits of other chelators.
- The bright deposits of all the copper electroless deposition baths show that the deposits are physically and mechanically good with roughness values lesser for glycerol counting to the fact that glycerol deposits are smoother than the other chelators.
- The CV, Tafel, and EIS studies also revealed that the deposition bath containing glycerol has given best results. This concludes that the bath with least number of hydroxides has given best results. This may be credited to the fact that with increase in bulkiness in the bath, the movement of ions are restricted which gets reflected in the bath performance.

4. Experimental Section

4.1. Materials

The chemicals were procured from the sources mentioned and used as such without further purification. Ethanol, ammonia solution (Fisher), copper methanesulphonate (S.D. Fine Chemicals), copper carbonate (Merck), glycerol, sorbitol, erythritol, and xylitol (Fisher), potassium hydroxide (Sigma–Aldrich), and dimethylamine borane (DMAB) (Merck). All stock solutions were prepared using double distilled water. The preparation of the stock solution and the pre-treatment of the substrate surface is shown in Flowchart S1 and S2.

4.2. Eco-Friendly Electroless Deposition Bath

The electroless deposition bath was prepared containing copper methanesulphonate as the metal ion, polyols as the chelator, and DMAB as the reducing agent. The methane sulphonic acids are the simplest of the alkylated sulphonic acids and has the chemical formula of CH_3SO_3H. Their conductivity made it a strong electrolyte which is comparable to the conductivity of strong acids like hydrochloric acid and sulphuric acid. Their conductivity is very much higher than most of the organic acids. Potassium hydroxide was used as the pH maintainer. The electroless baths containing glycerol, erythritol, xylitol, and sorbitol as chelator, each in four distinct baths were optimized at a pH of 11.50, 11.25, 11.0, and 10.75, respectively. The epoxy resin polymer sheet (2.0 × 2.0 × 0.1 cm) was used as the substrate, which was scrubbed, surface cleaned, pre-activated, and dipped in the electroless bath solution.[31–33] The bath composition of the electroless bath engaged is shown in Table S1.

4.3. Calculation of Deposition Rate and Thickness of Copper Deposits

The deposition rate of the electroless copper deposits can be calculated using the relation:

$$\text{Rate of deposition}\left(\frac{\mu m}{h}\right) = \text{Thickness} \times \text{Deposition time} \quad (1)$$

The thickness of the copper deposits can be calculated from the following relation:

$$\text{Thickness}\,(\mu m) = \frac{W \times 10^4 \times 60}{A \times D} \quad (2)$$

where W is weight of the deposit (g), A is total plated area of the substrate (cm^3), and D is density of the copper (8.96 g/cm^3).

4.4. Atomic Force Microscope (AFM)

The surface roughness of the copper deposits was analyzed using an atomic force microscope (AFM). It has a microfabricated cantilever, with an integrated tip mounted on a holder at the end of the cantilever. The operation of AFM is generally described in any of these modes: contact mode and non-contact mode. In these modes, the attractive and repulsive forces between the sample and the tip is measured. In contact mode, the tip at the end of the cantilever of the microscope slightly touches the sample. The hard-sphere repulsion force generated between the sample and the tip is measured. In non-contact mode, the tip does not touch the sample. The attractive force gives the topographic images of the sample. This approach can also be used to evaluate samples in liquids and

air with a resolution of 10 pm, which makes it unique from the other electron microscopes.

4.5. X-ray Diffraction (XRD) Studies

XRD technique can be used in the determination of crystal structure of solids. In the electroless deposition process, the structural properties of the deposited copper are identified by the XRD studies. Collimated monochromatic X-rays generated from a cathode ray tube is directed toward the sample. The interaction of incident rays with the sample, produces a constructive interference which obeys the Bragg's law.

$$\lambda = 2d \sin\theta$$

where "d" is the atomic planes spacing in the crystalline phase and "λ" is the X-ray wavelength.

The relationship between the wavelength of electromagnetic radiation, angle of diffraction, and lattice spacing of a crystalline sample can be obtained from the Bragg's relation. The sample is scanned through a range of 2θ angles. The diffracted rays will attain all the possible directions of the lattice, because of the random orientation of the material. These diffraction peaks will be converted in to d-spacings which give information about the material. The particle size of the deposits is calculated from the Debye–Scherrer equation.

$$D = K\lambda/\beta \text{rad} \cos\theta$$

where K is the Scherrer constant, λ is the wavelength of light used for the diffraction, β is the "Full Width Half Maximum"(rad) of the sharp peaks, and θ is the angle measured. The Scherrer constant (K), accounts for the shape of the particle and is given a value of 0.89.

4.6. Cyclic Voltammetry

The electrochemical behavior of a system can be investigated by the cyclic voltametric technique. The anodic peak potential and peak current values described the amount and quality of the deposits.[34,35] The voltammograms were captured in 0.1 M Na_2SO_4 supporting electrolyte at 28 ± 2 °C room temperature, with a 0.005 M concentration of DMAB and copper solution. The working electrode was a micro-disk of conventional glassy carbon electrode, and the potential scanning rate was 50 mVs^{-1}. Voltammograms were obtained in the range of −1.2 to + 0.5 V. KOH solution at varying pH was used to optimize the 0.1 M Na_2SO_4 supporting electrolyte solution for polyhydroxylic baths. The electrolyte concentration, nature of the electrodes and the sweep rates determines the height and width of the peak for a particular process.[36–38] Adsorption, diffusion, and the mechanism of the homogeneous coupled chemical reaction are discussed by the voltammogram's breadth, amplitude, and potential peaks.

4.7. DC Electrochemical Monitoring Technique – Tafel Polarization (TP)

This technique involves applying a voltage that is distant from the corrosion potential to a standard calomel electrode. The polarization curves for the anodic and cathodic reactions are then obtained by recording the current. Allow currents in the two Tafel zones to be extrapolated by plotting the logarithm of current (log I) against potential. The Tafel plot can be used to determine the reduction current of copper salts, which is equivalent to the oxidation current of the reducing agent, DMAB. The corrosion current (Icorr) allows one to compute the rate of corrosion using Faraday's law.

This polarization method involves varying the working electrode's potential and monitoring the current generated as a function of potential or time. In an electrochemical process, the electrons can either be created or consumed. The rate of electron flow is measured by the rate of reaction. The rate of corrosion is measured by the metal penetration rate or the weight loss per unit area. At + 0.1 V of the corrosion potential, the potential-current density curve is roughly linear. The corrosion current density is correlated with the polarization resistance, which may be found by calculating the slope of the linear component of the plot and is as follows:

$$R\rho = \frac{\beta_a \times \beta_c}{2.303\,(\beta_a + \beta_c)\,I_{corr}} \tag{3}$$

where βa and βc are the magnitudes of the anodic and cathodic Tafel lines of Tafel slopes, respectively, and Rp is the polarization resistance.

The rate of corrosion can be directly correlated with the corrosion current found using the Tafel plot. Compared to weight loss measurements, this approach yields faster and more reliable findings.

4.8. Electrochemical Impedance Spectroscopy (EIS)

The AC impedance method can be used to investigate the corrosion phenomenon in an electroless bath. The electrode perturbation is reduced and the electrochemical features of the surface corrosion process are acquired when a low amplitude oscillating potential is given to the working electrode. Using this potent method, metal-coated surfaces can be characterized. In this instance, the voltage drop at the interface between the working electrode and the electrolyte is measured when a voltage is applied between the working electrode and the counter electrode. As a result, the electrolyte and working electrode experience an interfacial charge transfer. The system is compatible with the analogous circuit below.

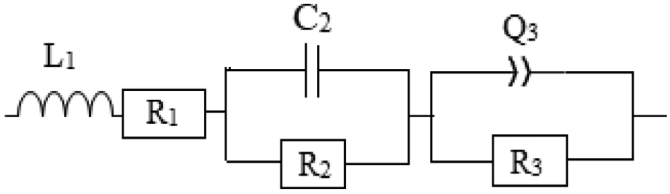

Where L_1 – Inductance, C_2 – Double layer capacitance, R_1, R_2, and R_3 – Resistances, and Q_3 – Constant phase element (imperfect capacitor).

$$Z_f = L_1\, i2\pi f + R_1 + \frac{R_2}{1 + i2\pi f R_2 C_2} + \frac{R_3}{R_3 Q_3 \left(i2\pi f\right)^{\alpha 3} + 1} \tag{4}$$

The imperfect capacitor utilized in the equivalent circuit is represented by the constant phase element, Q_3, whose value can be stated as C_2 (pseudo capacitance), which is derived from the Z-fit of the EIS spectrum. Applying a modest voltage—between 5 and 50 Mv—to a sample across a frequency range of 10 mHz to 50 kHz is how the EIS test is carried out. The impedance response's real and imaginary components are noted. The values of the inductance, charge transfer resistance, and double layer capacitance are determined using the EIS spectrum form, the circuit specifications, and the circuit description code.

Acknowledgements

This work was supported by the "2024 System Semiconductor Technology Development Program" funded by the Chungbuk Technopark. The authors also acknowledge and appreciate the Ongoing Research Funding Program (ORF-2025-774), King Saud University, Riyadh, Saudi Arabia.

Conflict of Interests

The authors declare no conflict of interest.

Author Contributions

Suseela Jayalakshmi: Investigation; writing—original draft. **Raja Venkatesan**: Formal analysis; methodology; investigation; writing—original draft. **Palanivelu Balaramesh**: Data curation; writing—review and editing. **Simon Deepa**: Conceptualization; data curation. **Maher M. Alrashed**: Validation; resources, funding acquisition. **Seong-Cheol Kim**: Supervision; project administration; writing—review and editing. All authors have read and agreed to the published version of the manuscript.

Data Availability Statement

The data that support the findings of this study are available from the corresponding author upon reasonable request.

Keywords: Copper deposition · Dimethylamine borane · Erythritol · Glycerol · Sorbitol · Xylitol

[1] A. Inberg, P. Livshits, Z. Zalevsky, Y. Shacham-Diamand, *Microelectron. Eng.* **2012**, *98*, 570–573.
[2] M. Paunovic, M. Schlesinger, in *Fundamentals of Electrochemical Deposition*, John Wiley & Sons, New York **2005**.
[3] H. Wang, N. Lin, M. Nouri, Z. Liu, Y. Yu, Q. Zeng, G. Ma, J. Fan, D. Li, Y. Wu, *J. Mater. Res. Technol.* **2023**, *27*, 6021–6046.
[4] S. Ghosh, *Thin Solid Films* **2019**, *669*, 641–658.
[5] C. Dehchar, I. Chikouche, R. Kherrat, A. Sahari, A. Zouaoui, A. Merati, *Mater. Lett.* **2018**, *288*, 439–442.
[6] R. H. Guo, S. Q. Jiang, C. W. M. Yuen, M. C. F. Ng, *J. Mater. Sci. Mater. Electron.* **2009**, *20*, 33-38.
[7] G. T. P. Azar, D. Fox, Y. Fedutik, L. Krishnan, A. J. Cobley, *Surf. Coat. Technol.* **2020**, *396*, 125971.
[8] A. Ojstršek, L. Jug, O. A. Plohl, *Polymers* **2022**, *14*, 4713.
[9] M. I. Hossain, S. Mansour, *Cogent. Eng.* **2023**, *10*, 2179467.
[10] L. E. Scriven, *MRS Proc.* **1998**, *121*, 717-729.
[11] H. Ding, B. Li, Z. Wang, S. Niu, Z. Han, L. Ran, *Matter* **2022**, *5*, 2990–3008.
[12] A. Lahiri, N. Borisenko, M. Olschewski, G. Pulletikurthi, F. Endres, *Faraday Discuss* **2018**, *206*, 339–351.
[13] G. Qin, Y. Zhang, M. Yuan, R. Chen, Y. Liu, J. Huang, *J. Mater. Sci.: Mater. Electron.* **2019**, *30*, 9767–9774.
[14] J. H. Huang, P. S. Shih, V. Renganathan, S. J. Gräfner, Y. A. Chen, C. H. Huang, C. L. Kao, Y. S. Lin, Y. C. Hung, C. R. Kao, *Electrochim. Acta* **2022**, *425*, 140710.
[15] P. Balaramesh, S. Jayalakshmi, S. A. Fdo, V. Anitha, P. Venkatesh, *Mater. Today Proc.* **2021**, *47*, 1862–1867.
[16] J. Huang, C. Tian, J. Wang, J. Liu, Y. Li, Y. Liu, Z. Chen, *Appl. Surf. Sci.* **2018**, *458*, 734–742.
[17] M. Georgieva, C. Girginov, M. Petrova, D. Lazarova, E. Dobreva, S. Kozhukharov, *Transactions of the IMF* **2021** *99*, 238–245.
[18] R. PauliukaitĖ, G. Stalnionis, Z. Jusys, A. Vaškelis, *J. Appl. Electrochem.* **2006**, *36*, 1261–1269.
[19] R. Fuchs-Godec, M. G. Pavlović, M. V. Tomic, *Int. J. Electrochem. Sci.* **2015**, *10*, 10502–10512.
[20] A. Sharma, C.-S. Cheon, J. P. Jung, *J. Microelectron. Packag. Soc.* **2016**, *23*, 1–6.
[21] A. Commarieu, W. Hoelderich, J. A. Laffitte, M.-P. Dupont, *J. Mol. Catalysis A. Chemical* **2002**, *182–183*, 137–141.
[22] M. A. Akhmedov, S. S. Khidirov, *Russ. J. Electrochem.* **2019**, *55*, 579–589.
[23] E. Norkus, A. Vaskelis, R. Pauliukaite, *Electroanalysis* **1999**, *11*, 447–449.
[24] L. D. Burke, R. Sharna, *J. Electrochem. Soc.* **2008**, *155*, D285.
[25] H. S. Magar, R. Y. A. Hassan, A. Mulchandani, *Sensors* **2021**, *21*, 6578.
[26] X. Qin, G. Lin, J. Wang, K. Zheng, X. Feng, *Prot. Met. Phys. Chem. Surf. 57*, 132–138.
[27] Y. Gan, J. D. Ong, S. K. Lee, T. W. Wan, S. C. Low, *J. Phys. Sci.* **2024**, *35*, 85–95.
[28] E. Barsoukov, J. R. Macdonald, Impedance Spectroscopy: Theory, Experiment, and Applications, Wiley, New York, **2005**.
[29] S. Jayalakshmi, R. Venkatesan, S. Deepa, A. A. Vetcher, S. Ansar, S.-C. Kim, *Sci. Rep.* **2023**, *13*, 11062.
[30] J. Cheng, L. Ding, Q. Li, C. Chen, R. Wang, X. Kong, Z. Song, X. Zhao, Y. Niu, *J. Appl. Electrochem.* **2020**, *50*, 475–488.
[31] F. C. Walsh, *Transactions of the IMF* **2022**, *100*, 233-244.
[32] R. R. Leleti, B. Hu, M. Prashad, O. Repič, *Tetrahedron Lett.* **2007**, *48*, 8505–8507.
[33] C. Uraz, S. Macit, *J. Eng. Sci.* **2018**, *20*, 369–375.
[34] J. Huang, Z. Sun, F. Zhou, Y. Yuan, W. Chen, M. Gao, Z. Chen, *J. Mater. Sci. Mater. Electron.* **2017**, *28*, 10974–10980.
[35] A. Dev, S. Tandon, P. Jha, P. Singh, A. Dutt, *Sādhanā* **2020**, *45*, 156.
[36] S. Danilova, J. E. Graves, G. V. W. Cave, J. Sort, E. Pellicer, A. J. Cobley, *Proc.* **2020**, *11324*, 1132412.
[37] N. Elgrishi, K. J. Rountree, B. D. McCarthy, E. S. Rountree, T. T. Eisenhart, J. L. Dempsey, *J. Chem. Educ.* **2018**, *95*, 197–206.
[38] L. Chen, R. K. L. Su, *Constr. Build. Mater.* **2021**, *267*, 121003.

Manuscript received: March 5, 2025